Intense high-harmonic optical vortices generated from a microplasma waveguide irradiated by a circularly polarized laser pulse

Ke Hu [1,2] and Longqing Yi [1,2,3,*]

[1] *Tsung-Dao Lee Institute, Shanghai Jiao Tong University, Shanghai 200240, China*
[2] *Collaborative Innovation Center of IFSA (CICIFSA), Shanghai Jiao Tong University, Shanghai 200240, China*
[3] *Key Laboratory for Laser Plasmas (Ministry of Education), School of Physics and Astronomy, Shanghai Jiao Tong University, Shanghai 200240, China*

(Received 19 February 2022; accepted 24 July 2022; published 2 August 2022)

A scheme for generating intense high-harmonic optical vortices is proposed. It relies on spin-orbit interaction of light when a relativistically strong circularly polarized laser pulse irradiates a microplasma waveguide. The intense laser field drives a strong surface wave at the inner boundary of the waveguide, which leads to high-order-harmonic generation as the laser is traveling inside. For a circularly polarized drive laser, the optical chirality is imprinted to the surface wave, which facilitates conversion of the spin angular momentum of the fundamental light into orbital angular momenta of the harmonics. A "shaken waveguide" model is developed showing that the aforementioned phenomenon arises due to a nonlinear plasma response that modifies the electromagnetic mode at high intensities. We further show that the phase velocities of all the harmonic beams are automatically matched to the driving laser, so that the harmonic intensities increase with propagation distance. The efficiency of harmonic production is related to the surface wave breaking effect, which can be significantly enhanced using a tightly focused laser. Our simulation suggests that an overall conversion efficiency of ∼5% can be achieved.

DOI: 10.1103/PhysRevResearch.4.033095

I. INTRODUCTION

Light can carry spin and orbital angular momenta (SAM and OAM) [1–3]. The SAM is related to the handedness of circular polarization, and a photon can carry SAM of $\sigma\hbar$, where $\sigma = -1$ or $+1$ for the left- or right-handed polarization, respectively. The OAM is possessed by light beams that exhibit helical wave fronts, which is typically expressed by a helical spatial phase $\exp(il\phi)$, where l is the topological charge and ϕ is the azimuthal angle. Recently, high-order-harmonic vortex sources have attracted considerable attention due to their applications in many fields of science, such as optical communication [4,5], optical trapping [6], and biophotonics [7]. Their special intensity profile makes them a useful tool to control laser-matter interactions [8–11].

Many studies have attempted to obtain intense, high-order vortex laser beams. It has been experimentally proven that a relativistic electron beam in a helical undulator can emit high-order strong vortex radiation [12,13]. In addition, Compton backscattering of a twisted laser from a gas target produces high-energy photons with OAM [14]. Another type of method that has promise is high-order-harmonic generation (HHG) from high-power lasers interacting with solid targets. Such approaches typically rely on HHG via the relativistic oscillating mirror (ROM) mechanism [15–17]; the driver can be a relativistic Laguerre-Gaussian (LG) beam [18,19], a tightly focused circularly polarized (CP) pulse [20,21], or a linearly polarized laser if plasma holograms are employed [22]. However, since the ROM mechanism is suppressed for CP drivers at normal incidence, it is challenging to generate intense circularly polarized vortex beams, which are of particular interest for controlling chiral structures [23,24] and optical manipulation at relativistic intensities [25].

Recently, we demonstrated [26] that high-harmonic optical vortices can also be generated when a high-power CP laser diffracts through a relativistic oscillating window (ROW). The laser drives chiral relativistic electron oscillations at the periphery of an aperture, which produces high-order harmonics via the Doppler effect and facilitates spin-orbital interaction of light. This could potentially boost the intensity of harmonic vortex beams since it no longer relies on the ROM mechanism. However, for typical plasma apertures (that can be produced by relativistic induced transparency [27–29], for example), which are a few times the laser wavelength in diameter, only the edge of the laser pulse near the periphery is responsible for HHG. This hinders achieving the goal of high laser-to-harmonics conversion efficiency.

In this paper, we show that the above obstacle can be tackled by irradiating a microplasma waveguide (MPW) with a relativistic CP laser. The interactions of lasers with such targets have already shown great potential in electron acceleration [30,31], radiation generation [32–35], production of ion beams [36,37] and manipulation of relativistic laser pulses [38]. Despite the progress that has been made in both theory

*lqyi@sjtu.edu.cn

and experiment [30], previous studies are mainly based on the linear theory of plasma waveguides [39], which fails to capture the modification of the electromagnetic mode due to the nonlinear plasma response on the boundary. Here, using first-order perturbation, we introduce a simple "shaken waveguide" model, which suggests that high-order harmonics are generated due to plasma oscillation on the inner wall, and the harmonic beams carry OAM if the drive laser is circularly polarized. Moreover, due to a phenomenon of self-phase-matching, this process continuously extracts energy from the drive laser, resulting in an overall conversion efficiency as high as 5%.

II. GENERATION OF HARMONIC VORTICES

We first demonstrate our scheme using a three-dimensional (3D) particle-in-cell (PIC) simulation with the EPOCH code [40]. The setup of laser-waveguide interaction is illustrated in Fig. 1(a). A CP driving laser pulse enters a cylindrical waveguide along the x axis from the left and travels to the right. The simulation box has dimensions of $x\times y\times z = 16\times14\times14\ \mu\text{m}^3$ and is sampled by $2400\times560\times560$ cells, with four macroparticles for electrons and two for C^{6+} per cell. A moving window is used to improve computational efficiency, which follows the propagation of the drive laser pulse in the MPW. The laser field is $\mathbf{E} = (\mathbf{e_y} + i\sigma\mathbf{e_z})E_0\exp(-r^2/w_0^2)\exp(-t^2/\tau_0^2)\exp(ik_0x - i\omega_0t)$, where $\mathbf{e_y}$ ($\mathbf{e_z}$) is the unit vector in the y (z) direction; E_0 is the laser amplitude; ω_0 is the angular frequency; $k_0 = 2\pi/\lambda_0$ is the wave number, with $\lambda_0 = 1\ \mu$m being the laser wavelength; $w_0 = 2.5\ \mu$m is the laser spot size; and $\tau_0 = 10.19$ fs, corresponding to a temporal full width at half maximum (FWHM) duration of 12.0 fs. The laser has a normalized amplitude $a_0 = eE_0/mc\omega_0 = 16$, where c is the speed of light, m is the electron mass, and e is the unit charge. In this simulation, the laser is right-handed circularly polarized ($\sigma = +1$). The MPW target has a length of $L = 100\ \mu$m, an inner radius of $r_0 = 5.0\ \mu$m, and a density of $n_0 = 30n_c$, where $n_c = \epsilon_0 m\omega_0^2/e^2$ is the critical density.

The laser energy is converted into waveguide modes when it enters the channel. Simultaneously, the relativistically strong CP laser field drives collective electron oscillations, forming a chiral surface wave that copropagates with the laser, as shown in Fig. 1(b). As the light bounces between such oscillating surfaces, it experiences a relativistic Doppler shift, which can lead to the generation of high-order harmonics [15,17].

The three-dimensional harmonic E_y fields ($\omega > 2.5\omega_0$) are shown in Fig. 1(a), which presents a helical structure known as a light spring [41]. This indicates that each harmonic frequency is associated with a spatial LG-like mode, and the topological number $l(\omega)$ varies linearly with ω. Such a structure is of particular interest for controlling the topology of laser-plasma accelerators [11].

In Figs. 1(c)–1(e), we show the field distribution of the second, third, and fourth harmonics in the cross section perpendicular to the propagation axis. One can see that the relation $l = (n-1)\sigma$ is satisfied in all cases, which is further confirmed by Fig. 1(f). The ratios of the longitudinal component of the total angular momentum

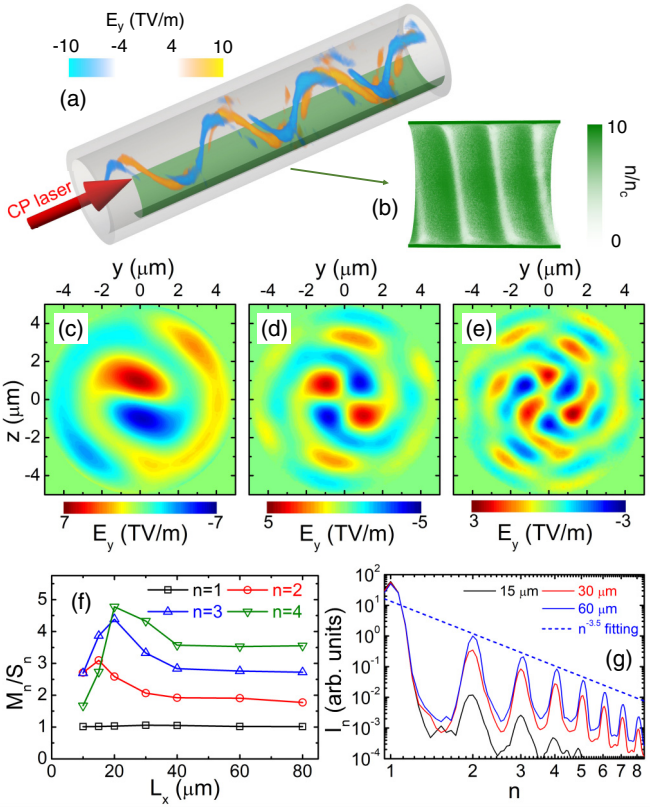

FIG. 1. (a) and (b) The 3D schematic setup of the proposed scheme. A circularly polarized laser pulse enters a MPW (gray tube) from the left, and high-order harmonics are generated as the light bounces between the channel walls (a), where a copropagating chiral surface wave driven by the laser is observed (b). The color-coded electric field E_y in (a) shows a light spring structure of the harmonic beams ($\omega > 2.5\omega_0$). (c)–(e) The E_y field distributions on the y-z cross section, for the second-, third-, and fourth-order harmonics, observed at propagation distance $L_x = 80\ \mu$m, respectively. (f) The ratio of total angular momentum to spin angular momentum plotted as a function of propagation distance for harmonics of order $n = 1$–4. (g) The spectra of the electromagnetic wave in the waveguide, observed at propagation distances of 15, 30, and 60 μm.

$M_n = \varepsilon_0[\int \mathbf{r}\times(\mathbf{E}_n\times\mathbf{B}_n)d\mathbf{r}]_x$ and the SAM $S_n = W_n/n\omega_0$ of the nth harmonic are plotted against propagation distance L_x for $n = 1$–4, where $\mathbf{E}_n$, $\mathbf{B}_n$, and W_n denote the electric field, magnetic field, and energy of the nth harmonic, respectively. Physically, this relation ensures the conservation of energy and angular momentum during the HHG process: The sum of the SAM of n fundamental-harmonic photons ($n\times\sigma\hbar$) is transformed into the SAM ($\sigma\hbar$) and OAM [$(n-1)\sigma\hbar$] of one nth-harmonic photon. We note that the left- or right-handedness of the drive CP laser only changes the sign of l for the generated harmonic vortices and has little effect on other results of this work; we therefore consider only the right-handed case $\sigma = +1$ hereinafter.

The harmonic spectra of the electromagnetic field observed at different propagation distances inside the MPW are illustrated in Fig. 1(g); the harmonic beams continuously extract energy from the driver for a few tens of micrometers. The HHG efficiency, defined as the energy of the harmonic beams

($n \geqslant 2$) over the total energy of the drive laser, is 3.64%. As for the harmonics in the VUV region (wavelength <200 nm), the efficiency is 0.32%. The spectra can be fitted with a power-law shape $I_n \propto n^{-3.5}$, where I_n is the intensity of the nth harmonics. This indicates that the HHG mechanism is very similar to that of the ROW [26]. This is expected because a waveguide can be considered as a train of coaxial diffraction apertures with the same radii. However, in our scheme, the chiral surface electron oscillation forms a copropagating surface wave, which is crucial for achieving a high conversion efficiency, as it allows for a long-time interaction between the drive laser and the oscillating surface electron layer.

III. SELF-PHASE-MATCHING EFFECT

The fact that harmonic intensities grow with propagation distance implies that they have the same phase velocity as the driver, such that harmonics generated at different longitudinal positions can add constructively. Previous work has shown that the harmonics are generated at the same angle with respect to the channel axis [42], but it is still unclear how they propagate afterwards. According to the plasma waveguide theory [32,39], the phase velocity is $v_{ph,n} = n\omega_0/k_{x,n}$, where $k_{x,n} = \sqrt{n^2k_0^2 - k_{T,n}^2}$, with $k_{T,n} = x_{1,n}/r_0$ being the transverse wave number and $x_{1,n}$ being the first root of the eigenvalue equation (here, we consider only fundamental waveguide modes). The subscript n denotes the nth harmonic. Since $x_{1,n}$ does not increase proportionally to n (in fact, it changes little with varying frequency [39]), one would expect that different orders of the harmonic beams would propagate at different velocities. As a result, the difference in phase velocities between the fundamental light and a high-order ($n > 10$) harmonic would potentially cause catastrophic negative interference within a few micrometers, which conflicts with the numerical results.

To explain the observed phenomena, we introduce a "shaken waveguide" model, taking into account the copropagating surface wave as a periodical deformation of the MPW. The center of the cross section is shifted by $\mathbf{\Delta} = -(\mathbf{e_y} + i\sigma\mathbf{e_z})\Delta_0 \exp(ik_x x - i\omega_0 t)$ due to collective electron oscillation, where the phase of the electron motion is opposite to the phase of the drive laser field. We take the linear plasma waveguide theory as the zeroth-order approximation [32,39], assuming that the cross section of the MPW remains circular and that the amplitude of this displacement Δ_0 is small, such that a perturbative method can be applied. The transverse electric field can be written as a sum of harmonics (see Appendix A),

$$\mathbf{E}_\perp = (\mathbf{e_y} + i\sigma\mathbf{e_z}) \sum_{n=1}^{\infty} E_0 \frac{J_0^{(n-1)}(k_T r)}{(n-1)!} (k_T \Delta_0)^{n-1} \times \exp[ink_x x - in\omega_0 t + i(n-1)\sigma\phi]. \quad (1)$$

We note that the intensities of harmonic beams cannot be obtained by the first-order perturbation unless the nonlinear term is small, i.e., $k_T \Delta_0 \ll 1$, which is not always true for the laser-plasma parameters under consideration. However, here we are mainly interested in the phase term of electromagnetic waves in the MPW. This term can be used to interpret the spin-orbital interaction of light that occurs during HHG, as well as the phase velocity modification of the harmonic beams. This is because the underlying physics, namely, the conservation law of angular momentum and the change of boundary condition, must always apply regardless of the strength of the nonlinearity.

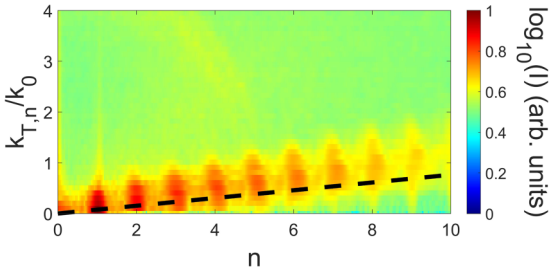

FIG. 2. 3D Fourier diagram of the E_y field in the waveguide, showing the intensity distribution of the generated harmonic beams in the k_T-ω space. The black dashed line is obtained by $k_{T,n}/k_0 = nx_1\lambda_0/2\pi r_c$.

One can see from Eq. (1) that the generated harmonic beams are circularly polarized with the same handedness as the driver and have helical phase fronts $\exp[i\sigma(n-1)\phi]$, from which the relation $l = (n-1)\sigma$ is recovered.

The deformation of MPW also modifies the boundary conditions, and consequently the propagation of the harmonic beams. In a "shaken waveguide," a longitudinal density modulation exists on the inner surface, with a period that is equal to the surface wave $2\pi k_x^{-1}$. Notably, Eq. (1) suggests that the longitudinal wave number for the nth-harmonic beam is $k_{x,n} = nk_x$; thus an integer number n of harmonic cycles exist between one surface wave crest [the dark parts in Fig. 1(b)]. In this way, the dynamical boundary condition is satisfied in all space and time, and therefore the phase velocities of all harmonic beams are locked with the driver.

This phenomenon of self-phase-matching is one of the key findings of this work and allows for a highly efficient production of the high-harmonic optical vortices. The result is further examined with 3D Fourier analysis of the E_y field observed at $L_x = 80$ μm in the y-t space (Fig. 2). The resulting intensity distribution in k_T-ω phase space shows a linear relation, which proves that all harmonics are propagating with the same phase velocity as the driving laser. The small deviation of the numerical results from the analytical relation $k_{T,n}/k_0 = nx_1\lambda_0/2\pi r_0$ is mainly because the phase velocity of the drive laser slightly differs from the theoretical value, as the laser has just entered the channel and it does not have time to fully transform into the fundamental waveguide mode.

IV. HHG EFFICIENCY ENHANCEMENT

In the following, we investigate the parameter dependence of the proposed HHG scheme and seek to improve the overall conversion efficiency for a given laser energy and a fixed MPW. The study is performed with 3D PIC simulations, and the parameters are the same as in Fig. 1 unless otherwise stated.

The general results are summarized in Fig. 3(a), where the ratio of laser waist to channel radius is set to be $w_0/r_0 = 0.5$

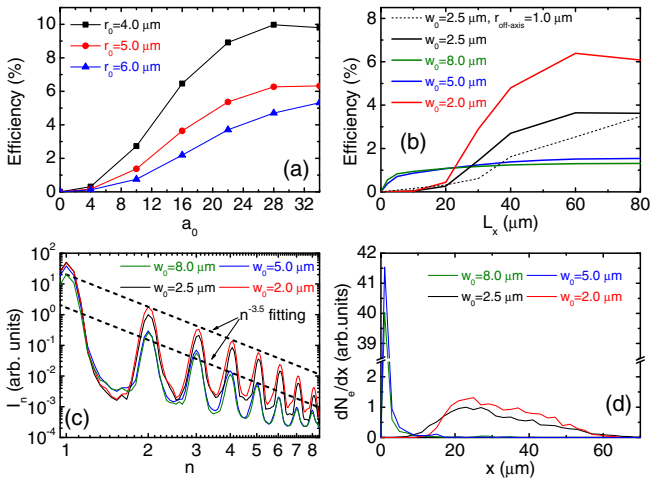

FIG. 3. (a) The HHG efficiency plotted as a function of a_0 for different r_0, where the laser waist w_0 is fixed at $r_0/2$. (b) The HHG efficiency plotted against propagation distance for a laser beam focused to different waists w_0 at the entrance of a MPW. The black dashed line shows the case of drive laser misalignment by 1 μm off axis. (c) The harmonic spectra observed at $L_x = 60$ μm, and (d) a histogram of the initial positions for the escaped high-energy electrons; the longitudinal position with high electron number count indicates where the SWB effect takes place. The total charges of injected electrons are 4.75, 5.12, 1.32, and 1.48 nC for $w_0 = 8.0$, 5.0, 2.5, and 2.0 μm, respectively. In (b)–(d) the laser energy is fixed to be 0.88 J, and the channel radius is $r_0 = 5.0$ μm for all cases.

(discussed below). One can see that when the laser is weak, the HHG efficiency increases rapidly with a_0, and then the slope becomes almost linear until it saturates at 5–10%. This trend is true for all the cases with different MPWs; however, the simulations suggest that for the waveguides with smaller radii, the efficiency slopes are steeper and saturate at lower driving intensities and typically slightly higher HHG efficiencies are obtained.

For practical reasons, it is of particular interest to optimize the drive laser for a given energy so that the harmonic vortices can be efficiently produced. Interestingly, we found that the HHG efficiency changes dramatically with varying waist-to-radius ratio w_0/r_0 in this situation.

The results are presented in Fig. 3(b), where four simulations are performed with laser waist $w_0 = 2.0$, 2.5, 5.0, and 8.0 μm, the drive energy is the same (the laser a_0 are adjusted accordingly), and the MPW radius is fixed at $r_0 = 5$ μm. One can see that when $w_0 \geqslant r_0$, almost all harmonics are generated near the entrance and the HHG intensities increase rapidly within the first few micrometers as the laser enters the MPW, but the HHG process terminates very soon ($L_x < 10$ μm), the energy of harmonic beams remains the same afterwards, and the efficiency is ~1%. On the other hand, when $w_0 < r_0$, the harmonics are mainly generated inside the channel and the intensities rise slowly in the beginning, but the process lasts for a much longer distance ($L_x \sim 60$ μm) and the HHG efficiency reaches ~5% in the end. We therefore conclude that a tightly focused laser can significantly enhance the HHG efficiency for the proposed scheme. Such a setup can be challenging for state-of-the-art laser systems due to the misalignment issue. Fortunately, our numerical results illustrate that the final HHG efficiency drops little due to a misalignment of magnitude of the order of 1 μm, as shown by the black dashed line in Fig. 3(b). Such a requirement of the pointing stability has been achieved in recent laser-waveguide experiments [30]. A preplasma also quantitatively reduces the overall efficiency (to ~1%); therefore a high-contrast laser is favorable for the scheme (see Appendix B).

The HHG spectra for the cases presented in Fig. 3(b) are shown in Fig. 3(c). Apparently, they all have a power-law shape that can be fitted with $I_n \propto n^{-3.5}$, while the harmonics produced by tightly focused drive lasers are several times stronger.

Since the high-order-harmonic vortices are generated through a similar mechanism with the ROW [26], namely, the chiral electron oscillation on the periphery of a high-power laser beam, the HHG efficiency depends crucially on the amplitude of the oscillation. A large amplitude is associated with the surface wave breaking (SWB) effect; that is, when the drive laser is sufficiently strong, some of the oscillating electrons acquire enough energy to escape, and they are ejected into the vacuum as energetic microbunches [43]. When SWB occurs, the surface wave is highly nonlinear, and its amplitude is at maximum; thus highly efficient HHG is expected. However, unlike the ROW, in our scheme the harmonic vortices are generated gradually as the laser pulse is propagating in the MPW; therefore achieving a high HHG efficiency requires the SWB effect to take place over a significant portion of the propagation distance.

How long the SWB effect can last is determined by the number of electrons that escaped. As more and more high-energy electrons are ejected into the vacuum, this in turn builds up a Coulomb barrier that prevents further electrons from escaping [34,35]. This ultimately suppresses SWB, leading to a reduction of the surface wave amplitude and, consequently, the HHG efficiency. In order to examine this effect, for each of the cases presented in Fig. 3(b), we track the trajectories of high-energy electrons ($\gamma > 10$) obtained at the end of the MPW and plot the histogram of their injection positions in Fig. 3(d). One can see that in all cases, the time at which high-harmonic intensities are rising rapidly coincides with the phase with SWB-induced electron injection, after which both the electron emission and the HHG process stop.

In the cases of $w_0 = 5.0$ and 8.0 μm, almost all energetic electrons are injected in the vicinity of the waveguide entrance. The strong impact of the laser pulse with the MPW front surface produces a large number of electrons. This effect is dominant for electron injection as long as the normalized laser intensity at the rim of the MPW is $a(r = r_0) \geqslant 1$. In this case, the Coulomb barrier is established within several micrometers, leading to a premature quenching of the HHG process.

In contrast, for $w_0 = 2.0$ and 2.5 μm, both cases satisfy that $a(r = r_0) \ll 1$, and the number of high-energy electrons originating from the entrance is negligibly small. The electron injection starts at around $L_x = 10.0$ μm and lasts up to $L_x = 60$ μm, during which the high-harmonic vortices are generated efficiently due to the lasting SWB effect. It should be noted that the number of high-energy electrons contributes little to the harmonic production; the electron emission is

merely a signature of the SWB effect. It is the distance over which electrons continue to emit that plays a vital role.

V. SUMMARY

In conclusion, we demonstrate that high-harmonic vortices can be generated with high overall efficiency up to ∼5% via an ultraintense CP laser irradiating a microplasma waveguide. A "shaken waveguide" model is introduced, which suggests that spin-orbital interaction of light takes place in the high-order-harmonic generation process when the drive laser pulse bounces between the channel walls, where a copropagating chiral surface wave is presented. The surface wave also modifies the boundary condition so that all the generated harmonic beams propagate with the same velocity as the drive laser pulse in the waveguide. This allows for constructive interference of the harmonic light generated along the propagation path. We show that a tightly focused laser beam is preferred for achieving a high overall efficiency, as it avoids massive electron injection near the entrance of the waveguide and therefore the amplitude of the surface wave can remain high for a long distance. Our study paves the way to realizing a powerful laser-plasma-based high-harmonic vortex source and provides theoretical insights into laser-waveguide interaction at ultrahigh intensities.

ACKNOWLEDGMENT

This work is supported by the National Key R&D Program of China (No. 2021YFA1601700), the Shanghai Pujiang Talent Plan (No. 21PJ1407500).

APPENDIX A: DERIVATION OF THE TRANSVERSE ELECTRIC FIELD IN A SHAKEN WAVEGUIDE

Based on the analytical model developed in Refs. [32,33,35,39], the radial and azimuthal components of the electric field in a waveguide are

$$E_r(x, r, \phi) \approx E_0 J_0(k_r r)\exp(i\sigma\phi)\exp(ik_x x - i\omega_0 t), \quad \text{(A1)}$$

$$E_\phi(x, r, \phi) \approx i\sigma E_0 J_0(k_r r)\exp(i\sigma\phi)\exp(ik_x x - i\omega_0 t). \quad \text{(A2)}$$

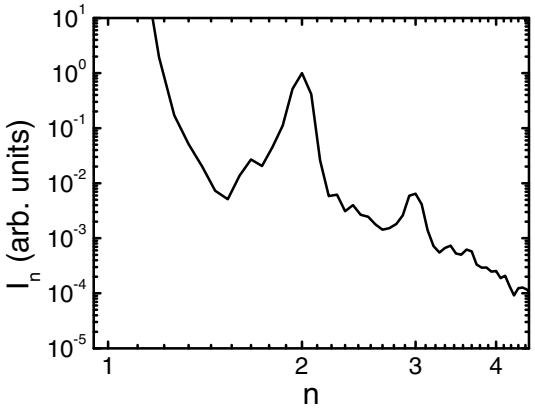

FIG. 4. Spectrum of the electromagnetic wave in a waveguide when the drive laser has amplitude $a_0 = 0.05$, obtained from a 2D PIC simulation. All parameters are the same as in Fig. 1.

The radial profile of the electric fields $[J_0(k_T r)]$ is an approximation, but this does not matter for the argument below (as long as it is some well-behaved function). Since we no longer have cylindrical symmetry in a shaken waveguide, we employ Cartesian coordinates:

$$\mathbf{E}_\perp = (\mathbf{e_y} + i\sigma\mathbf{e_z})E_0 J_0(k_T r')\exp(ik_x x - i\omega_0 t), \quad \text{(A3)}$$

where $r = \sqrt{y^2 + z^2}$ is measured from the original axis and $r' = \sqrt{y'^2 + z'^2}$ is measured from the axis of the deformed waveguide. Because the phase of electron motion is opposite to the local electric field, the shift of the axis in the y and z directions is given by $\delta y = -\Delta_0\exp(ik_x x - i\omega_0 t)$ and $\delta z = -i\sigma\Delta_0\exp(ik_x x - i\omega_0 t)$, respectively. The amplitudes are the same because of the symmetry of the setup. So we have

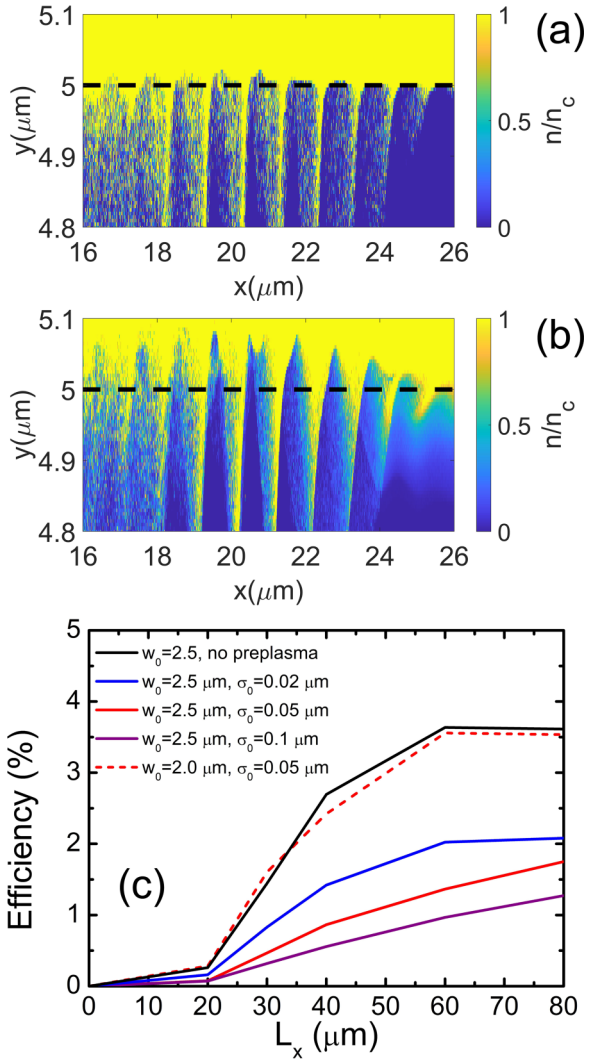

FIG. 5. (a) and (b) Yellow-blue color maps showing the distributions of density at the inner surface of the waveguide, with a sharp boundary (without preplasma) (a) and with preplasma (b). The snapshots are taken when the laser peak is at $x = 20$ μm. The black dashed line shows the initial inner boundary of the waveguide [where $n(r) = 1n_c$ for (b)]. (c) The efficiency of high-order-harmonic generation plotted against propagation distance for different preplasma scale lengths σ_0 and laser spot sizes w_0. The other parameters are the same as in Fig. 1.

$y' = y + \Delta_0 \exp(ik_x x - i\omega_0 t)$ and $z' = z + i\sigma\Delta_0 \exp(ik_x x - i\omega_0 t)$; thus $r' \approx r + \Delta_0 \exp(ik_x x - i\omega_0 t + i\sigma\phi)$. Substituting this into Eq. (A3) and performing Taylor expansion, one obtains

$$\mathbf{E}_\perp = (\mathbf{e_y} + i\sigma \mathbf{e_z}) \sum_{n=1}^{\infty} E_0 \frac{J_0^{(n-1)}(k_T r)}{(n-1)!} (k_T \Delta_0)^{n-1} \times \exp[ink_x x - in\omega_0 t + i(n-1)\sigma\phi], \quad \text{(A4)}$$

where $J_0^{(n-1)}$ represents the $(n-1)$th-order derivative of the Bessel function of the first kind. The helical phase term $\exp[i(n-1)\sigma\phi]$ illustrates that the spin-orbital interaction of light occurs during high-order-harmonic generation.

One may notice that the coefficient $(k_T \Delta_0)^{n-1}/(n-1)!$ in Eq. (A4) suggests that the harmonic intensities decrease very rapidly with harmonic order n. This is because the amplitude in Eq. (A4) is only accurate when $k_T \Delta_0 \ll 1$, namely, $a_0 \ll 1$. Figure 4 shows the spectrum for the case of $a_0 = 0.05$ from a 2D PIC simulation; the harmonics of $n > 3$ can hardly be observed. Therefore, in this paper, we only take into consideration the phase term of Eq. (A4). The underlying physics of the spin-orbit interaction of light and self-phase-matching, i.e., the conservation of total angular momenta and the modification of the phase velocities of the harmonic beams due to the surface wave, works the same way regardless of the intensity of the drive laser.

APPENDIX B: PREPLASMA EFFECTS

A preplasma at the inner surface of the waveguide quantitatively reduces the overall efficiency because in the low-density region, the boundary deformation due to the transverse laser ponderomotive force is significant. This effect may modify the phase velocity of the driver. Moreover, the boundary deformation depends on the intensity of the driver, which decreases with time, so the phase velocity of the driver is therefore time dependent. This leads to a small discrepancy in the phase-matching condition for harmonic beams produced at different times.

We ran a series of 3D simulations to investigate the effect of preplasma on our scheme. The density profile of the preplasma is $n(r) = n_0 \exp[(r - r_0)/\sigma_0]$, where σ_0 is the scale length. We can clearly observe the boundary deformation when a preplasma exists ($\sigma_0 = 0.05\ \mu$m), shown in Fig. 5(b), by comparing it with the case of no preplasma shown in Fig. 5(a). The conversion efficiencies for different scale lengths are plotted in Fig. 5(c). We can see that the increase in the preplasma scale length reduces the overall efficiency of harmonic generation. When the scale length is $\sigma_0 = 0.05\ \mu$m, the efficiency is about half of that in the case of no preplasma. Therefore a high-contrast drive laser is necessary to achieve >1% overall efficiency in the presented scheme.

We would like to emphasize that the key findings of our work persist when preplasma exists. (i) For all the cases presented in Fig. 5(c), the intensities of harmonic beams grow with propagation distance, indicating that the automatic phase matching between harmonic beams and the fundamental laser still plays a vital role. The aforementioned effects of preplasma only reduce the overall efficiency quantitatively. (ii) In general, high overall efficiency above 1% can be obtained. In particular, using a tightly focused drive laser remains an effective way to enhance HHG efficiency: From the red dashed line in Fig. 5(c) we see that when $\sigma_0 = 0.05\ \mu$m, the efficiency is almost doubled (3.5%) with a laser waist $w_0 = 2.0\ \mu$m compared with the efficiency obtained with $w_0 = 2.5\ \mu$m.

[1] L. Allen, M. W. Beijersbergen, R. J. C. Spreeuw, and J. P. Woerdman, Orbital angular momentum of light and the transformation of Laguerre-Gaussian laser modes, Phys. Rev. A **45**, 8185 (1992).

[2] A. M. Yao and M. J. Padgett, Orbital angular momentum: Origins, behavior and applications, Adv. Opt. Photon. **3**, 161 (2011).

[3] K. Y. Bliokh, F. J. Rodríguez-Fortuño, F. Nori, and A. V. Zayats, Spins orbit interactions of light, Nat. Photon. **9**, 796 (2015).

[4] J. Wang, J.-Y. Yang, I. M. Fazal, N. Ahmed, Y. Yan, H. Huang, Y. Ren, Y. Yue, S. Dolinar, M. Tur, and A. E. Willner, Terabit free-space data transmission employing orbital angular momentum multiplexing, Nat. Photon. **6**, 488 (2012).

[5] G. Gibson, J. Courtial, M. J. Padgett, M. Vasnetsov, V. Pas'ko, S. M. Barnett, and S. Franke-Arnold, Free-space information transfer using light beams carrying orbital angular momentum, Opt. Express **12**, 5448 (2004).

[6] A. T. O'Neil, I. MacVicar, L. Allen, and M. J. Padgett, Intrinsic and Extrinsic Nature of the Orbital Angular Momentum of a Light Beam, Phys. Rev. Lett. **88**, 053601 (2002).

[7] K. I. Willig, S. O. Rizzoli, V. Westphal, R. Jahn, and S. W. Hell, STED microscopy reveals that synaptotagmin remains clustered after synaptic vesicle exocytosis, Nature (London) **440**, 935 (2006).

[8] M. Onoda, S. Murakami, and N. Nagaosa, Hall Effect of Light, Phys. Rev. Lett. **93**, 083901 (2004).

[9] K. Y. Bliokh, A. Niv, V. Kleiner, and E. Hasman, Geometrodynamics of spinning light, Nat. Photon. **2**, 748 (2008).

[10] M. Padgett and R. Bowman, Tweezers with a twist, Nat. Photon. **5**, 343 (2011).

[11] J. Vieira, J. T. Mendonça, and F. Quéré, Optical Control of the Topology of Laser-Plasma Accelerators, Phys. Rev. Lett. **121**, 054801 (2018).

[12] E. Hemsing, A. Marinelli, and J. B. Rosenzweig, Generating Optical Orbital Angular Momentum in a High-Gain Free-Electron Laser at the First Harmonic, Phys. Rev. Lett. **106**, 164803 (2011).

[13] E. Hemsing, A. Knyazik, M. Dunning, D. Xiang, A. Marinelli, C. Hast, and J. B. Rosenzweig, Coherent optical vortices from relativistic electron beams, Nat. Phys. **9**, 549 (2013).

[14] U. D. Jentschura and V. G. Serbo, Generation of High-Energy Photons with Large Orbital Angular Momentum by Compton Backscattering, Phys. Rev. Lett. **106**, 013001 (2011).

[15] S. V. Bulanov, N. M. Naumova, and F. Pegoraro, Interaction of an ultrashort, relativistically strong laser pulse with an overdense plasma, Phys. Plasmas **1**, 745 (1994).

[16] R. Lichters, J. Meyer-ter-Vehn, and A. Pukhov, Short-pulse laser harmonics from oscillating plasma surfaces driven at relativistic, Phys. Plasmas **3**, 3425 (1996).

[17] T. Baeva, S. Gordienko, and A. Pukhov, Theory of high-order harmonic generation in relativistic laser interaction with overdense plasma, Phys. Rev. E **74**, 046404 (2006).

[18] X. Zhang, B. Shen, Y. Shi, X. Wang, L. Zhang, W. Wang, J. Xu, L. Yi, and Z. Xu, Generation of Intense High-Order Vortex Harmonics, Phys. Rev. Lett. **114**, 173901 (2015).

[19] A. Denoeud, L. Chopineau, A. Leblanc, and F. Quéré, Interaction of Ultraintense Laser Vortices with Plasma Mirrors, Phys. Rev. Lett. **118**, 033902 (2017).

[20] J. W. Wang, M. Zepf, and S. G. Rykovanov, Intense attosecond pulses carrying orbital angular momentum using laser plasma interactions, Nat. Commun. **10**, 5554 (2019).

[21] L. Zhang, B. Shen, Z. Bu, X. Zhang, L. Ji, S. Huang, M. Xiriai, Z. Xu, C. Liu, and Z. Xu, Vortex Harmonic Generation by Circularly Polarized Gaussian Beam Interacting with Tilted Target, Phys. Rev. Applied **16**, 014065 (2021).

[22] A. Leblanc, A. Denoeud, L. Chopineau, G. Mennerat, P. Martin, and F. Quéré, Plasma holograms for ultrahigh-intensity optics, Nat. Phys. **13**, 440 (2017).

[23] K. Toyoda, K. Miyamoto, N. Aoki, R. Morita, and T. Omatsu, Using optical vortex to control the chirality of twisted metal nanostructures, Nano Lett. **12**, 3645 (2012).

[24] K. Toyoda, F. Takahashi, S. Takizawa, Y. Tokizane, K. Miyamoto, R. Morita, and T. Omatsu, Transfer of Light Helicity to Nanostructures, Phys. Rev. Lett. **110**, 143603 (2013).

[25] W. P. Wang, C. Jiang, B. F. Shen, F. Yuan, Z. M. Gan, H. Zhang, S. H. Zhai, and Z. Z. Xu, New Optical Manipulation of Relativistic Vortex Cutter, Phys. Rev. Lett. **122**, 024801 (2019).

[26] L. Yi, High-Harmonic Generation and Spin-Orbit Interaction of Light in a Relativistic Oscillating Window, Phys. Rev. Lett. **126**, 134801 (2021).

[27] B. Gonzalez-Izquierdo, R. J. Gray, M. King, R. J. Dance, R. Wilson, J. McCreadie, N. M. H. Butler, R. Capdessus, S. Hawkes, J. S. Green, M. Borghesi, D. Neely, and P. McKenna, Optically controlled dense current structures driven by relativistic plasma aperture-induced diffraction, Nat. Phys. **12**, 505 (2016).

[28] B. Gonzalez-Izquierdo, M. King, R. J. Gray, R. Wilson, R. J. Dance, H. Powell, D. A. Maclellan, J. McCreadie, N. M. H. Butler, S. Hawkes, J. S. Green, C. D. Murphy, L. C. Stockhausen, D. C. Carroll, N. Booth, G. G. Scott, M. Borghesi, D. Neely, and P. McKenna, Towards optical polarization control of laser-driven proton acceleration in foils undergoing relativistic transparency, Nat. Commun. **7**, 12891 (2016).

[29] M. J. Duff, R. Wilson, M. King, B. Gonzalez-Izquierdo, A. Higginson, S. D. R. Williamson, Z. E. Davidson, R. Capdessus, N. Booth, S. Hawkes, D. Neely, R. J. Gray, and P. McKenna, High order mode structure of intense light fields generated via a laser-driven relativistic plasma aperture, Sci. Rep. **10**, 105 (2020).

[30] J. Snyder, L. L. Ji, K. M. George, C. Willis, G. E. Cochran, R. L. Daskalova, A. Handler, T. Rubin, P. L. Poole, D. Nasir, A. Zingale, E. Chowdhury, B. F. Shen, and D. W. Schumacher, Relativistic laser driven electron accelerator using micro-channel plasma targets, Phys. Plasmas **26**, 033110 (2019).

[31] K. D. Xiao, T. W. Huang, L. B. Ju, R. Li, S. L. Yang, Y. C. Yang, S. Z. Wu, H. Zhang, B. Qiao, S. C. Ruan, C. T. Zhou, and X. T. He, Energetic electron-bunch generation in a phase-locked longitudinal laser electric field, Phys. Rev. E **93**, 043207 (2016).

[32] L. Yi, A. Pukhov, P. Luu-Thanh, and B. Shen, Bright X-Ray Source from a Laser-Driven Microplasma Waveguide, Phys. Rev. Lett. **116**, 115001 (2016).

[33] L. Yi, A. Pukhov, and B. Shen, Radiation from laser-microplasma-waveguide interactions in the ultra-intense regime, Phys. Plasmas **23**, 073110 (2016).

[34] L. Yi and T. Fülöp, Coherent Diffraction Radiation of Relativistic Terahertz Pulses from a Laser-Driven Microplasma Waveguide, Phys. Rev. Lett. **123**, 094801 (2019).

[35] K. Hu, L. Yi, and T. Fülöp, Multimillijoule terahertz radiation from laser interactions with microplasma waveguides, Plasma Phys. Controlled Fusion **63**, 035028 (2021).

[36] D. B. Zou, A. Pukhov, L. Q. Yi, H. B. Zhuo, T. P. Yu, Y. Yin, and F. Q. Shao, Laser-driven ion acceleration from plasma microchannel targets, Sci. Rep. **7**, 42666 (2017); **7**, 44956(E) (2017).

[37] T. Kluge, S. A. Gaillard, K. A. Flippo, T. Burris-Mog, W. Enghardt, B. Gall, M. Geissel, A. Helm, S. D. Kraft, T. Lockard, J. Metzkes, D. T. Offermann, M. Schollmeier, U. Schramm, K. Zeil, M. Bussmann, and T. E. Cowan, High proton energies from cone targets: Electron acceleration mechanisms, New J. Phys. **14**, 023038 (2012).

[38] L. L. Ji, J. Snyder, A. Pukhov, R. R. Freeman, and K. U. Akli, Towards manipulating relativistic laser pulses with micro-tube plasma lenses, Sci. Rep. **6**, 23256 (2016).

[39] H. Shen, Plasma waveguide: A concept to transfer electromagnetic energy in space, J. Appl. Phys. (Melville, NY) **69**, 6827 (1991).

[40] T. D. Arber, K. Bennett, C. S. Brady, A. Lawrence-Douglas, M. G. Ramsay, N. J. Sircombe, P. Gillies, R. G. Evans, H. Schmitz, A. R. Bell, and C. P. Ridgers, Contemporary particle-in-cell approach to laser-plasma modelling, Plasma Phys. Controlled Fusion **57**, 113001 (2015).

[41] G. Pariente and F. Quéré, Spatio-temporal light springs: Extended encoding of orbital angular momentum in ultrashort pulses, Opt. Lett. **40**, 2037 (2015).

[42] S. V. Bulanov, T. Zh. Esirkepov, N. M. Naumova, and I. V. Sokolov, High-order harmonics from an ultraintense laser pulse propagating inside a fiber, Phys. Rev. E **67**, 016405 (2003).

[43] N. Naumova, I. Sokolov, J. Nees, A. Maksimchuk, V. Yanovsky, and G. Mourou, Attosecond Electron Bunches, Phys. Rev. Lett. **93**, 195003 (2004).